Autodetachment from vibrational levels of the O− 2 A 2Π u resonance across its dissociation limit by photoexcitation from O− 2 X 2Π g

Christopher G. Bailey, David J. Lavrich, David Serxner, and Mark A. Johnson

Citation: The Journal of Chemical Physics **105**, 1807 (1996); doi: 10.1063/1.472056
View online: http://dx.doi.org/10.1063/1.472056
View Table of Contents: http://scitation.aip.org/content/aip/journal/jcp/105/5?ver=pdfcov
Published by the AIP Publishing

Autodetachment from vibrational levels of the O_2^- $A\,^2\Pi_u$ resonance across its dissociation limit by photoexcitation from O_2^- $X\,^2\Pi_g$

Christopher G. Bailey, David J. Lavrich, David Serxner, and Mark A. Johnson
Department of Chemistry, Yale University, 225 Prospect Street, P.O. Box 8107, New Haven, Connecticut 06520-8107

(Received 15 February 1996; accepted 22 April 1996)

We report the observation of resonance structure in the photodetachment spectrum of O_2^- in the 4 eV range, which results from the excitation of autodetaching vibrational levels of the O_2^- $A-X$ transition near the dissociation limit. The evolution of the resonances with increasing vibration is simply explained using continuity of the inner part of the vibrational wave functions across the dissociation threshold. This affords the possibility of investigating the DA process at the half-collision, in a kind of ''correspondence limit'' where the outer turning point slowly recedes and the vibrational wave function incrementally adopts the character of the dissociation continuum. Photoexcitation near one of the resonances results in the population of significantly higher vibrational levels in the O_2 $a^1\Delta_g$ state (which are cleanly resolved) than the typical ''Franck–Condon'' pattern observed for nonresonant photodetachment. Finally, hot-band structure is also observed in the detachment spectrum, allowing us to extract a more accurate value of the O_2^- vibrational quantum ($\Delta G = 134.4 \pm 0.8$ meV) by about an order of magnitude over previous determinations. © *1996 American Institute of Physics.* [S0021-9606(96)00129-8]

I. INTRODUCTION

Negative ion photodetachment [i.e., photodetachment (action) and fixed excitation frequency (photoelectron)] spectroscopies are rapidly becoming the tools of choice in the vibrational characterization of negative ions and their associated neutral molecules.[1,2] In most applications, structural parameters can be extracted from vibrational band contours under the assumption that Franck–Condon factors govern the intensities of the vibrational features. It is clear, however, that this assumption is not valid when the photon creates a transient negative ion, $[A^-]^*$,

$$A^- + h\nu \rightarrow [A^-]^* \rightarrow A + e^- \tag{1}$$

with sufficient lifetime to allow finite motion of the nuclei before the state decays into a free electron and neutral molecule.[3] Examples of such transient negative ions are the *shape* and *Feshbach* resonances extensively studied in inelastic electron–molecule scattering.[4] Very recently, we demonstrated that the vibrational pattern associated with scattering through the shape resonance in CH_3CN^- at 2.9 eV is reflected in the photoelectron spectrum of the CH_3CN^- dipole-bound anion upon photodetachment in the vicinity of the resonance.[5] In the CH_3CN case, the resonance is so broad ($\sim$1 eV) that vibrational structure is not resolved in the transient negative ion. In this paper, we report the first observation of vibrational fine structure in the photodetachment spectrum of O_2^-, and demonstrate that when O_2^- is photodetached near one of the resonant features, the O_2 $a^1\Delta_g$ vibrational progression extends far beyond the Franck–Condon envelope. We trace these effects to autodetachment in the O_2^- $A\,^2\Pi_u$ excited electronic state, where the potential exists as a core-excited Feshbach resonance at small internuclear distances. These results are discussed in the context of analogous phenomena observed in inelastic electron scattering experiments involving N_2.[6]

A. Review of transient negative ions and electron scattering

The scattering of electrons by the ground electronic states of molecular oxygen and nitrogen has played a central role in the development of the theory of vibrationally inelastic electron–molecule interactions.[7] This theory[8–11] describes the nature of transient negative ions whose potential energy curves (see Fig. 1) evolve with internuclear distance, R, from a stable region through a ''crossing'' with the neutral surface, where the localized state mixes with the electron continuum (dashed extensions of the curves in Fig. 1) and generally autodetaches with a rate, $\Gamma(R)$. This state-mixing mediates the capture of the free electrons into molecular orbitals when anions are formed in the dissociative attachment (DA) process. In the case of O_2, low energy electrons are captured in the π_g LUMO to form bound O_2^- in the $X\,^2\Pi_g$ ground electronic state. The autodetachment rate for this state is sufficiently slow that the decaying electronic resonance supports vibrational motion of the anion, which can be observed as structure in the kinetic energy dependence of the inelastic electron scattering cross sections.[6] The O_2^- $X\,^2\Pi_g$ transient negative ion is principally formed from the $\pi_u^4\pi_g^3$ configuration, which can decay back to the ground state of neutral O_2 in a simple one-electron process. Therefore, the finite lifetime of the $X\,^2\Pi_g$ state results from a shape resonance in which the electron is temporarily trapped due to the high angular momentum barrier associated with the ($l \approx 2$) π_g^* LUMO orbital.[12]

Electronically excited states of anions can also possess such crossings with the potential curves of the neutral. For example, the formation of O^- in DA of O_2 is thought to

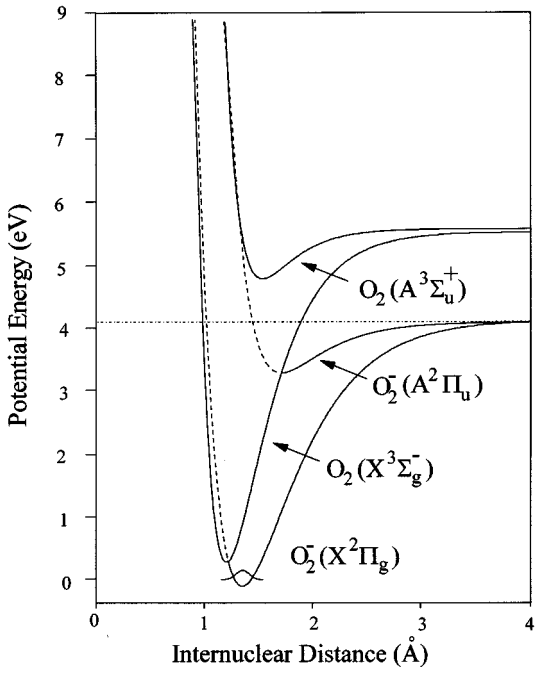

FIG. 1. Morse potentials for the O_2^- $X\ ^2\Pi_g$ and $A\ ^2\Pi_u$ states as well as their parent O_2 states, $X\ ^3\Sigma_g^-$ and $A\ ^3\Sigma_u^+$ respectively. The dashed portion of the curves indicates regions of the O_2^- potentials that are unstable with respect to autodetachment.

occur via the O_2^- $A\ ^2\Pi_u$ excited state.[13] The O^- resonance occurs[13] at about 7 eV, which is readily understood in the context of the potential curves (Morse forms)[14] shown in Fig. 1. The $A\ ^2\Pi_u$ state is generated by the promotion of a π_u electron to form the $\pi_u^3\pi_g^4$ electron configuration,[15] and as such is derived from the $\pi_u^3\pi_g^3$ parent configuration of neutral oxygen. The lowest O_2 term arising from this excited configuration is the $A\ ^3\Sigma_u^+$ state, 4.4 eV above ground state O_2, so that O_2^- $A\ ^2\Pi_u$ lies below its parent neutral state as shown in Fig. 1. Therefore, the $A\ ^2\Pi_u$ state must decay by two-electron processes

$$O_2^-(A\ ^2\Pi_u) \rightarrow O_2(X,a,b) + e^- \tag{2}$$

to the O_2 (X, a, or b) states corresponding to the ground $\pi_u^4\pi_g^2$ configuration. These considerations indicate that the $A\ ^2\Pi_u$ electronic state of the anion decays as a Feshbach resonance,[4] unlike the shape resonance encountered in the decay of the $X\ ^2\Pi_g$ O_2^- ground state.

B. Strategy of the present experiments

From the relative displacements of the curves in Fig. 1, it is clear that vertical electron attachment onto neutral O_2 occurs to a very repulsive region of the O_2^- $A\ ^2\Pi_u$ potential (about 3 eV above the dissociation asymptote) and the DA spectrum indeed consists of a broad, structureless feature.[13] However, O_2^- $A\ ^2\Pi_u$ can be *optically* prepared[14] much lower in energy than is possible in the DA process. In fact, photoexcitation of the $A\ ^2\Pi_u$–$X\ ^2\Pi_g$ transition from $X(v=0)$ has maximum vibrational overlap at the inner repulsive wall of the A state near the O_2^- dissociation limit. In an earlier publication,[16] we reported that photoexcitation of the O_2^- A–X band leads to O^- photofragments with a quantum yield of about 3%, placing an upper bound on the rate for the direct coupling of $A\ ^2\Pi_u$ to the continuum of about 3×10^{14} s^{-1}. The Franck–Condon region of the $A(v)$–$X(v=0)$ transition should also access *bound* vibrational levels of the A state, however, and in this paper we use optical spectroscopy to monitor the behavior of these $A\ ^2\Pi_u$ vibrational levels as they merge into the dissociative continuum. We are primarily interested in following the evolution of the DA process *across* the dissociation threshold, where the $A(v)$ vibrational levels are coupled to the *electron* continuum through the decay of the $A\ ^2\Pi_u$ ''potential'' at the inner turning point of the vibration. This affords the possibility of investigating the DA process at the half-collision, in a kind of ''correspondence limit'' where the outer turning point slowly recedes, and the vibrational wave function incrementally adopts the character of the dissociation continuum.

II. EXPERIMENT

Superoxide anion, O_2^-, is prepared by secondary electron attachment following high energy electron impact ionization at the throat of a supersonic expansion of oxygen seeded in helium or argon (4–6 atm), depending on the internal temperature required for various experiments (see Sec. III E). Bare O_2^- is mass selected and photoexcited using a pulsed laser/time-of-flight strategy described previously.[17] Photons in the range 3.85 to 4.15 eV were obtained by frequency doubling the signal beam from an optical parametric oscillator (Spectra Physics MOPO-710) pumped by the third harmonic of an injection-seeded Nd:YAG laser. Three experiments were performed to define the dynamics of the $A\ ^2\Pi_u$ state

$$O_2^-(X\ ^2\Pi_g) + h\nu \rightarrow O_2(X,a,b) + e^- \tag{3}$$

$$\rightarrow O_2^-(A\ ^2\Pi_u) \rightarrow O^- + O \tag{4a}$$

$$\rightarrow O_2(X,a,b) + e^-, \tag{4b}$$

where Eq. (3) represents direct detachment (i.e., ''normal'' photoelectron spectroscopy) and Eqs. (4a) and (4b) describe the two decay pathways of the O_2^- $A\ ^2\Pi_u$ state: dissociation and autodetachment to neutral (bound, for excitation below 6 eV) O_2. First, the threshold for process (4a) is monitored using tandem TOF mass spectroscopy to isolate the O^- product as a function of laser excitation energy. In a second experiment, the total photodetachment cross section is monitored by the production of fast O_2 (and, above the dissociation threshold, O atom) photoneutrals, which are easily detected with microchannel plates since they are created at high velocity corresponding to the kinetic energy of the parent ion beam (3.5 keV). The parent ions are deflected toward the detector prior to photoexcitation, so that the background neutral O_2 hitting the detector is negligible (<5% of the photoinduced signal), and the spectrum in Fig. 2(b) results after subtraction of this background. Finally, the decay

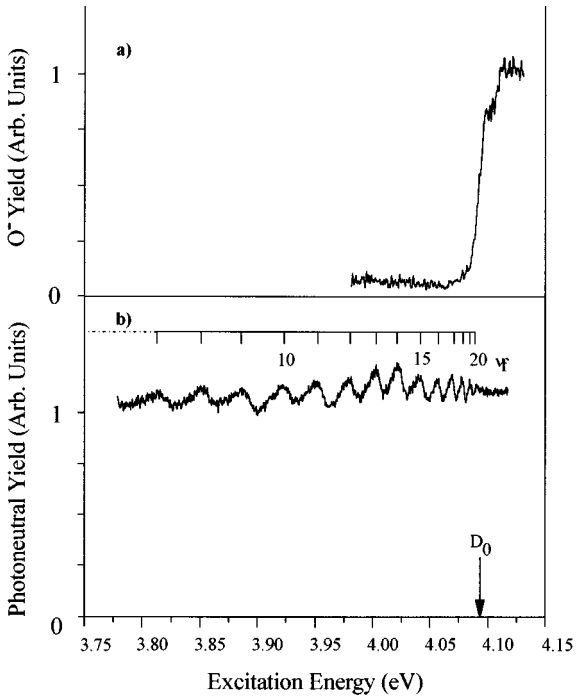

FIG. 2. Action spectra for excitation of the O_2^- $A-X$ transition obtained by detecting (a) the O^- photofragments, and (b) the fast neutral (O_2 molecules and, above the dissociation energy, D_0, O atom) photofragments.

pathways of an individual vibrational resonance are established by dispersing the autodetached electron [Eq. (4b)] in a field-free, time-of-flight photoelectron spectrometer. A ''control'' photoelectron spectrum was also taken by carrying out photodetachment with a photon energy well below region of the resonances (3.497 eV) to establish the vibrational patterns resulting from direct detachment [Eq. (3)]. For both cases (on and off resonance), photoelectron spectra were recorded with both parallel and perpendicular polarizations (relative to the electron drift axis) to establish the electronic state assignments of the vibrational features.

III. RESULTS AND DISCUSSION

A. Observation of resonances in the O_2^- $A-X$ spectrum below the dissociation threshold

Figure 2(a) presents the O^- photofragment action spectrum, which displays a relatively sharp onset in the region just above the O_2^- dissociation limit ($D_0=4.09$ eV).[18] The small tail to lower energy is dependent on source conditions and hence the rotational temperature of the ions, a point which is discussed in more detail in Sec. III E. The fast-neutral action spectrum was also scanned over this threshold region with the results presented in Fig. 2(b). This photodetachment spectrum is structured, consisting of a progression of features superimposed on a large background, with the features accounting for about 5% modulation of the total neutral yield. The presence of these peaks just below the dissociation energy of ground state O_2^- suggests their assignment to high vibrational levels of the $A\ ^2\Pi_u$ state in the $A-X$ electronic transition. This was checked by calculating the energies expected for high vibrational levels using published Morse parameters for the $A\ ^2\Pi_u$ state,[19] which confirmed that the spacing and compression of the features converging on the dissociation limit are as anticipated for $A\ ^2\Pi_u$ vibrational levels in the range $10 \leqslant v \leqslant 20$. The vibrational features are clearly broadening toward lower vibrational quantum number, and the pattern is lost before the origin is observed so that the absolute numbering could not be established. We therefore expect that the error in the absolute vibrational assignment is on the order $\Delta v = 1$ or 2.

B. Simple model for vibrational dependence of electronic autodetachment

Two aspects of the vibrational progression are readily apparent: the asymmetric peak shapes, where each member has a fast falling edge toward higher excitation energy, and the *narrowing* of the features as they approach the dissociation limit. This narrowing indicates that the autodetachment rates are decreasing for the vibrational levels on the verge of the dissociation limit. The near-constant heights of the vibrational features in Fig. 2(b) is interesting in light of the fact that the widths are changing so rapidly. This implies that the areas of the bands (and hence absorption cross sections, σ_v) are falling in proportion to their widths (i.e., autodetachment rates, Γ_v). Similar behavior was found by Heutz *et al.*[20] in their study of the vibrational features observed in inelastic electron scattering in N_2 near the dissociation threshold of N_2^-.

The overall structure of the O_2^- photodetachment spectrum [Fig. 2(b)] can be understood on an intuitive level in the context of the potential curves sketched in Fig. 3, which isolates the region of the crossings between the O_2^- $A\ ^2\Pi_u$ state and the three low lying states of neutral O_2. Included in the figure are a few representative vibrational wave functions obtained from the Morse potential approximation for the $A\ ^2\Pi_u$ potential. These are not normalized so that the entire shape of each representative wave function can be seen. Clearly, near the top of the well, the strong anharmonicity of the potential causes most of the wave function to be displaced toward the outer turning point. Thus, the probability of finding the system in the region of inner turning point ($R<R_e$) is rapidly decreasing near the dissociation limit. On the other hand, the exact shape of the wave function near the inner wall is not changing for the last few vibrational levels since they are quite close in energy, and the vibrational states primarily differ by their behavior at the outer turning point. In this respect, the problem is reminiscent of a Rydberg series (defined by principle quantum number, n) where electronic wave functions have similar shapes near the core but are weighted with a normalization factor, $\mathbb{N}^2 \propto 1/n^3$, so that the absorption cross section to a particular n level decreases as $1/n^3$. Recall that the normalization factor is related to the level density $[\mathbb{N}^2 \propto (dn/dE)^{-1}]$, however, such that absorption is continuous across the ionization threshold ($1/n^3 \cdot dn/dE \approx$ constant). Allison and Delgarno[21] have shown that an analogous rule applies to the case of photoab-

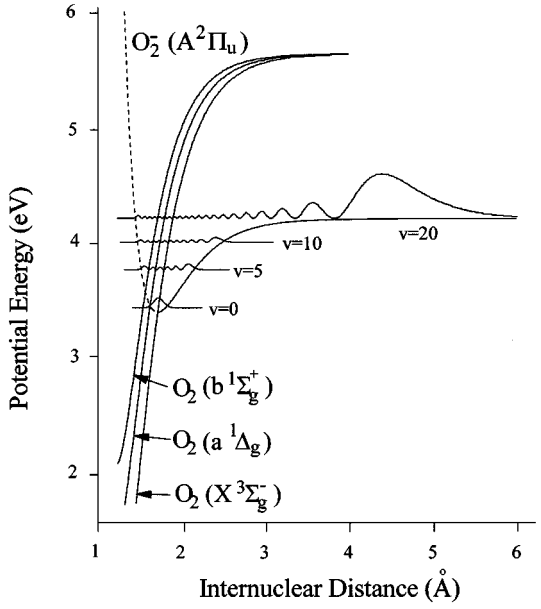

FIG. 3. The region of the crossing between the three low lying electronic states of O_2 and the $A\ ^2\Pi_u$ excited state of O_2^-, along with selected vibrational wave functions obtained by solving the Schrodinger equation using the Morse parameters (ω_0=592 cm^{-1}, D_0=0.77 eV, R_e=1.69 Å) for the $A\ ^2\Pi_u$ state. The wave functions are not normalized so that the entire shape of each can be readily compared, especially in the region $R<2$ Å.

sorption across the high vibrational levels into the dissociation continuum. The cross section to the dissociation continuum, σ_c, is related to the *integrated* cross section for excitation of the last vibrational level, σ_{vL}, as

$$\sigma_c = \sigma_{vL}\frac{dv}{dE}, \tag{5}$$

where dv/dE is the vibrational level density. Allison and Stwalley[22] traced the physical origin of this dependence to the fact that the period of the vibration increases at the top of the well due to the time spent at the outer turning point, while the time at the inner turning point, which ''determines'' the absorption spectrum, is nearly the same in this energy region. With this in mind, it is useful to break the vibrational wave function at the top of the well into two parts

$$\chi_v(R) \sim \mathbb{N}_v\{\chi_{\rm in}(R<R_e) + \chi_{\rm out}^v(R>R_e)\}, \tag{6}$$

where $\chi_{\rm in}(R<R_e)$ is a *normalized* wave function describing the inner region of internuclear separation, R, below the equilibrium distance of the A state, R_e. This wave function is approximately constant as $v \to v_L$, while the vibrational dependence is carried by the outer wave function, $\chi_{\rm out}^v(R>R_e)$, and the normalization constant, $\mathbb{N}_v$. Equation (5) implies that $\mathbb{N}_v^2$ is proportional to $(dv/dE)^{-1}$, so that the decrease in χ at the inner turning point (evident in Fig. 3 at high v) is expressed in Eq. (6) by the vibrational dependence of the normalization constant. The value of this treatment in our case is that it highlights the fact that the shape of the (v independent) wave function at the inner turning point, $\chi_{\rm in}(R<R_e)$, determines the important overlap integrals for absorption to *and* decay of excited levels of the $A\ ^2\Pi_u$ state so that the vibrational dependence is governed only by the level density.

The observed asymmetric peak shapes in Fig. 2(b) are expected when a discrete vibrational state, Φ_v, interacts with the continuum, Ψ_E, to yield a line shape for absorption from the ground state, Ψ_0, with the usual (i.e., ''Fano'') functional form[23]

$$\sigma(\epsilon_v) = \frac{(q+\epsilon_v)^2}{1+\epsilon_v^2}, \tag{7}$$

where q is defined through

$$\tfrac{1}{2}\pi q^2 = \frac{|\langle\Psi_0|r|\Phi_v\rangle|^2}{\Gamma_v|\langle\Psi_0|r|\Psi_E\rangle|^2} \tag{8}$$

and thus represents the ratio of the transition moments to the discrete and continuum states (scaled by the decay rate, Γ_v), and ϵ_v

$$\epsilon_v = \frac{h\nu - E_{\rm res}(v)}{(1/2)\Gamma_v} \tag{9}$$

denotes the excitation energy, $h\nu$, relative to the location of the vibrational resonance, $E_{\rm res}(v)$, in units of the decay rate.

In the case of the O_2^- $A\ ^2\Pi_u$ state, the absorption cross section to a discrete vibrational state v [numerator in Eq. (8)] from the ground (X) state is governed by

$$\sigma_v \propto |\langle\Psi_0|r|\Phi_v\rangle|^2. \tag{10}$$

At high v, this matrix element scales as $\mathbb{N}_v^2$ since the Franck–Condon overlap between the A state vibronic level, Φ_v, and the ground state [$X(v=0)$] is dominated by the v independent, $\chi_{\rm in}(R<R_e)$ contribution to χ_v so that $\langle\Psi_0|r|\Phi_v\rangle \propto \mathbb{N}_v\langle\chi_{\rm in}|\chi_0\rangle$. [Note that Eq. (10) applies to the case where $\Gamma(R)$ is sufficiently slow that the vibrational level is explored on the time scale of the resonance; the more general case involves the effective vibrational wave function, $\xi(R)$, for the resonant state which can be calculated[11] by propagating the ground vibrational state in a complex potential.] Within the simple model, however, the autodetachment rate of the A state vibrational level χ_v can be expressed as

$$\Gamma_v \propto \sum_{v'} |\langle\chi_v|\zeta(R)|\chi_{v'}\rangle|^2, \tag{11}$$

where $\chi_{v'}$ denotes all the final state neutral levels, v', populated upon autodetachment, and $\zeta(R)^2[\propto\Gamma^A(R)]$,[11] is the electronic operator coupling the resonant state and final continuum states. Once again, at high vibrational levels, the $\langle\chi_v|\zeta(R)|\chi_{v'}\rangle$ matrix elements in Eq. (11) are determined by the inner vibrational wave function $\chi_{\rm in}$ [Eq. (6)] since the three target electronic states of neutral O_2 ($X\ ^3\Sigma$, $a\ ^1\Delta$, $b\ ^1\Sigma$) possess vibrational wave functions which are significant only at internuclear separations less than R_e of the O_2^- A state (in the energy range near the O_2^- dissociation limit, see Fig. 3). In this case, $\mathbb{N}_v^2$ factors out of each summand in Eq. (11) and $\Gamma_v \propto \mathbb{N}_v^2$.

Thus at the top of the potential well, the absorption coefficient to a vibrational level and its decay rate are linked in that both scale as $\mathbb{N}_v^2$. Furthermore, since $\mathbb{N}_v^2 \propto dE/dv$, the

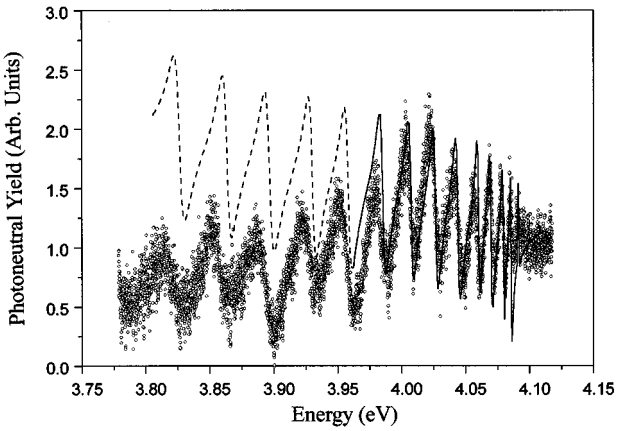

FIG. 4. Experimental detachment spectrum overlaid with simulated spectrum using Eqs. (7)–(12) with the values $q=-1$ and $\Gamma_0=0.22$ for the entire series.

vibrational dependence of the line shapes are *controlled by the level spacing,* and the behavior of all the levels near the dissociation limit are governed by the absorption cross section and decay rate of any particular level. Like a converging Rydberg series, the absorption cross sections, σ_v, to successively higher levels fall off in exactly the same way as the decay rates (and hence widths) of the levels, Γ_v, as the levels grow closer together near the top of the well. This nicely explains the qualitative appearance of the spectrum [Fig. 2(b)] where the vibrational levels get sharper as they come closer together such that they display roughly the same overall peak intensity. This can be made more quantitative by testing whether the vibrational dependence of the autodetaching rates can be fit with a form

$$\Gamma_v=\frac{dE}{dv}\Gamma_0, \tag{12}$$

where Γ_0 is the rate defined by the shape of χ_v from Eqs. (6) and (11). Figure 4 presents the detachment spectrum expected from this model in the limit where each resonance is treated separately and convoluted to simulate the spectrum, and both σ_v and Γ_v scale as dE/dv. Given the simplicity of the model, the stimulated spectrum reproduces the observed trend remarkably well with values $q=-1$ and $\Gamma_0=0.22$. The agreement is especially good over the highest ten vibrations or so, indicating that the essential physics is indeed captured by Eqs. (6) and (10)–(12). The direction of the asymmetry of each resonance dictates that q have a negative value, while the shapes of the peaks (rather distorted, somewhat removed from the location of the unperturbed resonant state) requires that the magnitude of the q parameter be much greater than zero. The fact that q is insensitive to vibrational level (i.e., constant for the series) derives from the fact that the denominator in Eq. (8) (direct detachment) is nearly constant while both the transition moment in the numerator and Γ_v in the denominator scale as dE/dv. The q value only pertains to the particular continuum state which is mixing with $A\ ^2\Pi_u$, however, and there is also a substantial contribution from the direct excitation of background continua. This direct detachment accounts for about 95% of the absorption cross section, so that the peaks appear as a small modulation of the net detachment background.

Note that the *shapes* of the lower vibrational levels are still actually well recovered with this simple treatment (dashed region in Fig. 4), although the predicted intensities are larger than the observed values. This is not unexpected, since the entire vibrational wave function becomes important at lower levels, and the χ_v approximation in Eq. (6) becomes increasingly poor. There is a sharp, downward peak in the simulated spectrum on the highest vibrational level, however, which is not present in the data. This may arise from the fact that the simulation does not include the contribution from the dissociation continuum below D_0; the simultaneous treatment of continua from both the electronic and nuclear degrees of freedom is beyond the scope of this paper, which primarily offers a rationalization of the effect rather than a definitive theoretical treatment.

C. Connection between the autodetaching resonances and the photodissociation quantum yield

Since the experimentally derived q value provides the ratio between the detachment cross section to the interacting continuum, σ_e, and that for excitation of the unperturbed bound state, σ_v, and Eq. (5) relates σ_v to the dissociation cross section, σ_c, it is possible to directly extract the quantity

$$\frac{\sigma_c}{\sigma_e}=\frac{\pi q^2}{2}\frac{\Gamma_{vL}}{dE/dv|_{vL}}=\frac{\pi q^2}{2}\Gamma_0, \tag{13}$$

where Γ_{vL} is the decay rate of the highest vibrational level and $dE/dv|_{vL}$ is the vibrational interval at the top of the well. Note that in this treatment, these values are related to Γ_0 via Eq. (12), so that two parameters, q, and Γ_0 define the evolution of cross section into the continuum. Insertion of experimental values, $\{|q|\approx 1,\ \Gamma_{vL}/[dE/dv]_{vL}[\equiv\Gamma_0$ in Eq. (12)$]\approx 0.22\}$, yields the ratio $\sigma_c/\sigma_e\approx 0.34$. Recall that σ_e pertains only to the interacting electron continuum, which is about 5% of the total continuum cross section, σ_e^{Tot}. We finally arrive at an estimate for the fraction, ϕ_{abs}, of the total absorption cross section which corresponds to excitation of the $A\ ^2\Pi_u$ state in the dissociation continuum, $\phi_{\mathrm{abs}}\approx(0.05)\times(0.34)\approx 2\%$, which compares remarkably well with the observed quantum yield for production of O^- above threshold, $\phi_{\mathrm{diss}}=3\%\pm 1\%$ [see Fig. 2(a)].

The agreement between ϕ_{abs} and ϕ_{diss} might, at first, appear fortuitous, since it implies that all excitation to the $A\ ^2\Pi_u$ results in fragmentation. One might assume that the fragmentation quantum yield would be bound from above by ϕ_{abs}, since surely ''pieces'' of the wave packet which start out with $R<R_e$ would be lost due to electron ejection. In this respect, it is useful to remember that the continuity of absorption strength across the dissociation threshold described by Eq. (5) also contains the implicit meaning that just above threshold, the initial vibrational wave packet must resemble the last vibrational level. Thus, most of the continuum packet

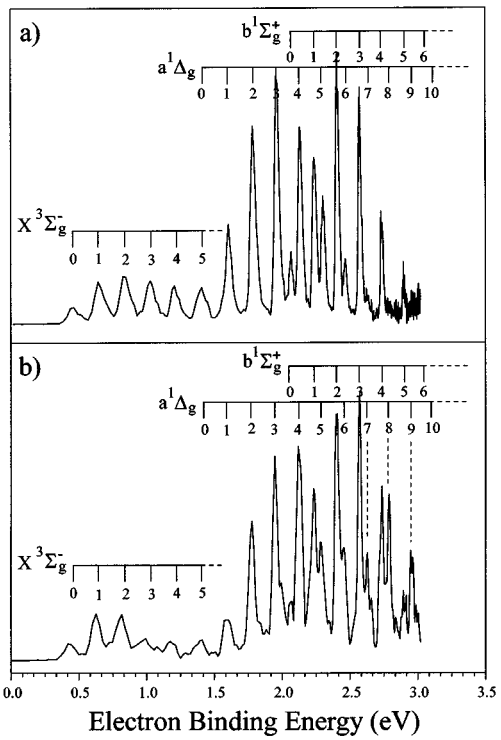

FIG. 5. Photoelectron spectra of O_2^- $X\ ^2\Pi_g$ at (a) 3.497 eV excitation energy and (b) 3.969 eV excitation energy close to the $v=12$ resonance in the $A\ ^2\Pi_u$ state.

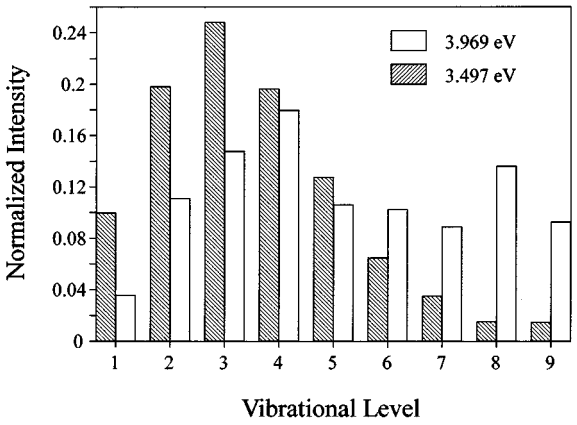

FIG. 6. Bar graph of the deconvoluted vibrational peak heights of the $a\ ^1\Delta$ state from the PES spectra in Fig. 5. The sum of the peak areas from each spectrum is normalized to unity. The shaded bars represent the nonresonant PES spectrum taken at 3.497 eV excitation, while the unshaded bars represent the resonant spectrum taken at 3.969 eV.

is launched from *beyond* R_e! With this in mind, it is clear that $\phi_{\text{abs}} \approx \phi_{\text{diss}}$ is expected on qualitative grounds.

D. Decay pathways of the $A\ ^2\Pi_u$ state: Non-Franck–Condon intensities in the photoelectron spectrum

An important consequence of autodetachment is its impact on the vibrational envelopes of photoelectron spectra when a resonance is excited, since the system can evolve on the anionic surface for a finite time before the electron is ejected. In the oxygen case, this evolution involves elongation of the bond length on the $A\ ^2\Pi_u$ ''potential'' curve, which should result in the population of higher vibrational levels than those formed in direct detachment. To investigate this process, we obtained photoelectron spectra resulting from excitation directly to a resonance [$v=12$ in Fig. 2(b)] and far from the resonances, at $h\nu=3.497$ eV.

The two photoelectron spectra are shown in Fig. 5, with upper trace displaying the nonresonant case and the lower arising from excitation of the $v=12$ resonance. Note that both spectra are quite similar at first glance, with the overlapping, Gaussian-shaped envelopes for each of the low lying states of O_2 (X,a,b). The nonresonant spectrum (a), can be recovered reasonably well with a fit to Franck–Condon factors using Morse functions for all the states. Very close inspection of the high electron binding energy region of the resonant spectrum [Fig. 5(b)] however, indicates that very high levels of the $a\ ^1\Delta$ state are populated ($v>6$) which are quite weak in the nonresonant spectrum. These peaks display much more symmetrical angular distributions than those displayed by the lower vibrational levels of the $X\ ^3\Sigma$ manifold, (asymmetry parameter, $\beta \ll 0$), which might be expected for autodetached electrons. They occur at the energies expected for high vibrational levels of $a\ ^1\Delta$ ($v=7$–9), however, which are clearly distinct from the nearby levels of the X and b states, and so we assign them to the $a\ ^1\Delta$ electronic state. We note that the asymmetry parameters of the new levels are very similar to those of the lower $a\ ^1\Delta$ vibrational levels. As the high vibrational levels of $X\ ^3\Sigma$ are blended with levels from the other states at our resolution, we cannot make a definitive statement about the vibrational distribution in the ground state. The $b\ ^1\Sigma$ levels are close to the low kinetic energy cutoff of the spectrometer, so that only levels $v<6$ of the a state could be cleanly observed in the spectrum.

To clarify changes in the $a\ ^1\Delta$ pattern, we have isolated the peak areas arising from this transition by fitting the overlapping bands and normalizing the sum of the areas of the peaks in each spectrum, with the results displayed as histograms in Fig. 6. The shaded bars correspond to the nonresonant spectrum, while the unshaded bars display the $a\ ^1\Delta$ vibrational pattern from resonant excitation. The $v=6$, 7, 8, and 9 peaks are much stronger in the resonant spectrum, indicating that the effect of the resonance is to elongate the vibrational progression beyond the bell-shaped Franck–Condon envelope. This behavior is again similar to that observed in N_2^- when the $A\ ^2\Pi_u$ state is excited as a transient negative ion by electron scattering and decays back to the ground state

$$e^- + N_2 \rightarrow N_2^-(A\ ^2\Pi_u) \rightarrow N_2(X\ ^1\Sigma)(v) + e^-, \tag{14}$$

where the vibrational distribution in the X state is very extended out to $v=30$ or so.[20]

Perhaps the most striking aspect of the resonance photoelectron spectrum is that the non-Franck–Condon peaks are actually a small fraction of the spectrum; at first glance the resonant and nonresonance spectra appear to be the same.

This is expected from our simple model, since autodetachment should be governed by χ_{in} of the A state [see Eq. (15)], which lies directly over the ground state $X\ ^2\Pi_g$ vibrational wave function. This indicates that the vibrational overlaps for direct detachment and autodetachment should be similar, with each creating extensive O_2 vibration. Another aspect which leads to similar spectra results from the fact that the resonances appeared only as a small modulation of the photodetachment spectrum, indicating that most of the detachment occurs to background states which are not involved in the autodetachment process. This background should have the usual pattern, and only 5% or so of the photoelectron quantum yield should participate in the resonant behavior. This implies that selective detection of one of the resonant features (such as $v=8$ of the $a\ ^1\Delta$) in photodetachment would yield very large modulations in the detachment spectrum, similar to the photoionization case in which action spectra are recorded for production of a particular state of the product ion.[24]

E. Hot band structure in the $A-X$ spectrum: Rotational effects and determination of the O_2^- $X\ ^2\Pi_g$ vibrational quantum

The presence of relatively sharp vibrational structure in the autodetachment spectrum affords the opportunity to obtain the location of the O_2^- $X\ ^2\Pi_g$ $(v=1)$ energy level through hot band structure in the autodetachment resonances. The shape of the O^- photodissociation spectrum can be used as a crude indication of the rotational temperature of O_2^- $X\ ^2\Pi_g$ $(v=0)$. Consider a system where only $J=0$ is occupied. Transitions from this single level to the excited state will yield O^- fragments with a sharp onset beginning at the bond dissociation energy D_0. For a system on the verge of dissociation, the rotational constant of the excited state is much less than that of the ground state ($B_{ex} \ll B_0$) and therefore the ground state rotational levels dominate the shift in excitation energy for photodissociation. Under these conditions, higher J levels in the ground state are dissociated at a lower excitation energy than $J=0$ by roughly $B_0 J(J+1)$. At excitation energy $E=B_{0\,\min}(J_{\min}+1)$ below threshold, all rotational levels $J>J_{\min}$ contribute to the cross section with intensity $2J+1$

$$\sigma \propto \sum_{J=J_{\min}}^{\infty} (2J+1) e^{-B_x J(J+1)/kT} \rightarrow e^{-B_x J_{\min}(J_{\min}+1)/kT}. \quad (15)$$

Thus a slow onset in the O^- action spectrum should conform to a simple Boltzmann distribution of rotational energy in a thermal ensemble of O_2^- parents.

The solid spectrum in Fig. 7 was acquired by photodissociation of O_2^- prepared with a stagnation pressure of ~6 atm He. The O^- action spectrum rises relatively sharply from the baseline, at $D_0(O_2^-)=4.09$ eV, consistent with a cold rotational temperature. The dotted spectrum in Fig. 7 was obtained from an equal mixture He and Ar at a stagnation pressure of 4 atm, showing a slower onset. Interestingly, both spectra display a shoulder at about 4.10 eV whose origin is unknown. These curved onsets were fit to Boltzmann distributions to estimate rotational temperatures of 65 and 125 K, respectively (smooth curves in Fig. 7).

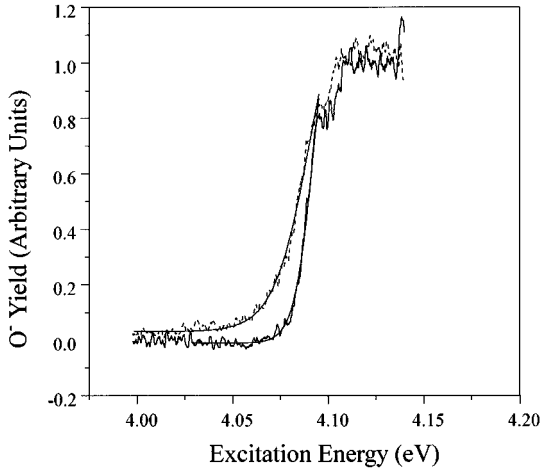

FIG. 7. Photodissociation action spectrum showing the dissociation threshold of O_2^- $A\ ^2\Pi_u$. The dotted curve is the spectrum from ''hot'' O_2^- prepared by backing the pulsed valve with a He/Ar mixture (see the text). The solid curve is the spectrum from ''cold'' O_2^- prepared by backing the pulsed valve with 6 atm He. The thick solid lines are Boltzmann fits to the data using Eq. (18).

An analogous temperature effect can also be used to generate vibrational hot bands. The $v=1$ quantum of O_2^- $X\ ^2\Pi_g$ has been previously measured by Ellison[25] (using photoelectron spectroscopy) to be 133 ± 6 meV. Earlier, Schulz[26] estimated a value of 132 meV by extrapolation

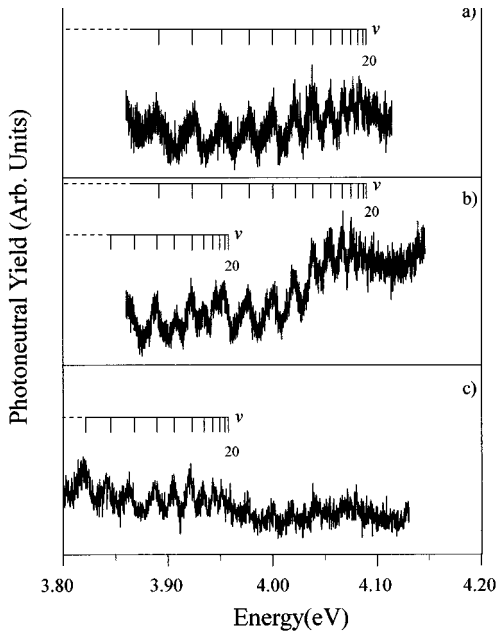

FIG. 8. Photodetachment spectra of O_2^- showing the evolution of the $A-X$ vibrational resonances with increasing vibrational temperature. The spectra are taken at (a) the coldest source conditions (~6 atm He stagnation pressure), (b) intermediate source conditions (~2 atm He), and (c) the hottest source conditions (0.5 atm Ar).

TABLE I. Experimentally determined ΔG_{01} values for O_2^-.

Reference no.	Method	$\Delta G_{01}(\mathrm{cm}^{-1})$
25	Photoelectron spectroscopy	1073±50
26	Electron scattering	1065
27	Raman spectroscopy	1090
28	Electron scattering	1137
This work	Autodetachment	1084±6

from higher vibrational features observed in electron scattering of O_2, and Bernstein[27] extrapolated the value of 135 meV from Raman spectra of O_2^- anions trapped in salt crystals.

The upper trace, (a), in Fig. 8 reproduces the vibrational progression from the coldest source condition (6 atm He stagnation pressure behind the nozzle) achieved in the present experiments, while the middle and lower spectra result from incrementally increasing the internal energy of the ions by lowering the stagnation pressure in the source. The middle spectrum, Fig. 8(b), appears complex as a new set of features is seen growing in at lower excitation energy relative to the main sequence shown in Fig. 2(b). This second set of features becomes dominant in the hottest spectrum displayed in the bottom trace [Fig. 8(c)], which is again simple as the original progression is barely observable in the presence of the hot band. The peak spacing uniquely identifies this second progression as sharing a common upper level with those in the primary progression. Each vibrational band is shifted by roughly 130 meV, clearly indicating that the second progression is a hot band arising from $v=1$ levels of the ground $X\ ^2\Pi_g$ state by comparison with earlier estimates of the quantum.

The dominance of the $v=1$ band over that from $v=0$ indicates that the Franck–Condon factors for the hot band transition are significantly larger than those arising from $v=0$. We therefore calculated the Franck–Condon factors from the Morse wave functions ($\omega_0=592\ \mathrm{cm}^{-1}$, $D_0=0.77$ eV, $R_e=1.69$ Å for the A state),[16] which indeed indicate that the hot bands to high v upper levels are much more intense (by a factor of 3 or so). Having assigned the hot band sequence, we obtained a best ΔG_{01} value from the line centers extracted from the ''Fano'' line shapes. The sharpest peaks ($v'>17$) were used to obtain an average vibrational term (ΔG_{01}) value of 134.4±0.8 meV, which is compared to previous values in Table I.

IV. CONCLUSIONS

Vibrational resonances are observed in the photodetachment spectrum of O_2^- which correspond to excitation of the $A-X$ transition in the bound region of the potential just on the verge of dissociation. This ''bound'' region is unstable with respect to autodetachment, however, as the electronic state supporting vibration decays as a Feshbach resonance. The vibrational dependence of the decay rate is consistent with a simple model built in analogy with decaying Rydberg series, where the absorption and decay processes are controlled by a normalization constant which depends on the level density. Analysis of the resonances recovers the observed quantum yield for photodissociation into $O+O^-$. The photoelectron spectra of O_2^- are affected by excitation in the neighborhood of a resonance. The effect is most clearly evident in the well-resolved $a\ ^1\Delta$ manifold, where a much longer vibrational progression is observed relative to that expected from Franck–Condon factors. Finally, vibrational hot bands are observed and analyzed to yield a more precise determination of the O_2^- $X(v=1)$ vibrational quantum ($\Delta G_{01}=134.4\pm0.8$ meV).

ACKNOWLEDGMENTS

The authors thank Professor W. A. Chupka and Dr. C. E. Klots for valuable discussions about relevant literature, P. Ayotte for his critical evaluation of the molecular physics, and Professor M. A. Buntine for early contributions to the work. Special thanks are owed to Professor W. C. Lineberger and Dr. M. Pollack for sharing their unpublished photoelectron data on the isovalent S_2^- anion. We thank the National Science Foundation for the support of this research.

[1] R. R. Corderman and W. C. Lineberger, Ann. Rev. Phys. Chem. **30**, 347 (1975).
[2] D. M. Neumark, Acc. Chem. Res. **26**, 33 (1993).
[3] E. Illenberger, Chem. Rev. **92**, 1589 (1992).
[4] I. Shimamura and K. Takayanagi, *Electron–Molecule Collisions* (Plenum, New York, 1984), p. 382.
[5] C. G. Bailey, C. E. Dessent, and M. A. Johnson, J. Chem. Phys. **104**, 6976 (1996).
[6] G. J. Schultz, Rev. Mod. Phys. **45**, 423 (1973).
[7] A. Herzenberg, in *Electron-Molecule Collisions* (Plenum, New York, 1984), p. 191.
[8] W. Domcke, J. Phys. B **14**, 4889 (1981).
[9] J. P. Gauyacq and A. Herzenberg, J. Phys. B **17**, 1115 (1984).
[10] J. N. Bardsley, J. Phys. B **1**, 349 (1968).
[11] R. I. Hall and F. H. Read, in *Electron–Molecule Collisions* (Plenum, New York, 1984), p. 378.
[12] K. J. Reed, A. H. Zimmerman, H. C. Andersen, and J. I. Brauman, J. Chem. Phys. **64**, 1368 (1976).
[13] R. J. Van Brunt and L. J. Kieffer, Phys. Rev. A **2**, 1899 (1969).
[14] A. M. Ikezawa and J. Rolfe, J. Chem. Phys. **58**, 2024 (1973).
[15] G. Das, A. C. Wahl, W. T. Zemke, and W. C. Stwalley, J. Chem. Phys. **68**, 4252 (1978).
[16] D. J. Lavrich, M. A. Buntine, D. Serxner, and M. A. Johnson, J. Chem. Phys. **99**, 5910 (1993).
[17] M. A. Johnson and W. C. Lineberger, in *Techniques in Chemistry*, edited by J. M. Farrar and W. H. Saunders, Jr. (Wiley, New York, 1988), Vol. 20, p. 591.
[18] K. P. Huber and G. Herzberg, *Molecular Spectra and Molecular Structure. IV. Constants of Diatomic Molecules* (Van Nostrand Reinhold, New York, 1979).
[19] J. Rolfe, J. Chem. Phys. **70**, 2463 (1979).
[20] A. Heutz, I. Cadez, F. Gresteau, R. I. Hall, D. Vichon, and J. Mazeau, Phys. Rev. A **21**, 622 (1980).
[21] A. C. Allison and A. Dalgarno, J. Chem. Phys. **55**, 4342 (1971).
[22] A. C. Allison and W. C. Stwalley, J. Chem. Phys. **58**, 5187 (1973).
[23] U. Fano Phys. Rev. **124**, 1866 (1961).
[24] J. Berkowitz, *Photoabsorption, Photoionization and Photoelectron Spectroscopy* (Academic, New York, 1979).
[25] M. J. Travers, D. C. Cowels, and G. B. Ellison, Chem. Phys. Lett. **164**, 449 (1989).
[26] D. Spence and G. J. Schulz, Phys. Rev. A **2**, 1802 (1970).
[27] J. Rolfe, W. Holzer, W. F. Murphy, and H. J. Bernstein, J. Mol. Spectrosc. **26**, 543 (1968).
[28] R. L. Gray, H. H. Haselton, D. Krause, Jr., and E. A. Soltysik, Chem. Phys. Lett. **13**, 51 (1972).